Sr $5p_{1/2}ns_{1/2}$ and $5p_{3/2}ns_{1/2}$ $J=1$ autoionizing states

Emily Y. Xu, Yifu Zhu, Oliver C. Mullins, and T. F. Gallagher
Department of Physics, University of Virginia, Charlottesville, Virginia 22901
(Received 23 September 1985)

We report a comprehensive experimental study of the Sr I autoionizing $5p_{1/2}ns_{1/2}$ and $5p_{3/2}ns_{1/2}$ $J=1$ states with n ranging from 10 to 36. We have used an isolated-core-excitation method to determine the energies, autoionization rates, and interseries interaction between the two $5p_{1/2}ns_{1/2}$ and $5p_{3/2}ns_{1/2}$ channels. A six-channel multichannel-quantum-defect-theory analysis of the data has been performed, and good agreement between the experiment and the theory has been obtained.

I. INTRODUCTION

The existence of autoionizing states has been known for 60 years, yet until recently they have remained a subject of largely academic interest. The increased current interest is due to two factors. First, it has been appreciated that autoionizing states can play an important role in applications such as lasers and plasmas.[1,2] Second, new theoretical and experimental techniques have been developed which are making the study of autoionizing states a far more quantitative process. On the theoretical side *ab initio* techniques such as many-body perturbation theory[3] and the random-phase approximation[4] have been developed which allow the calculation of the crucial atomic parameters. In parallel, quantum defect theory[5,6] has been developed which allows the reduction of different types of experimental data to a few parameters which can be calculated by *ab initio* theory.

Experimentally, the advent of synchrotron light sources and tunable dye lasers has led to substantial advances. Of specific interest here is the use of multistep dye laser excitation techniques in which several "single-electron" transitions are driven.[7] This makes it possible to readily identify the configurations of the observed autoionizing states, not simply their angular momentum and parity. Furthermore, by using such an approach only the autoionizing state is excited with negligible continuum excitation so that the observed autoionizing resonance is free of the usual Beutler-Fano interference[8] allowing the positions and widths to be taken directly from the data. This simplification is crucial in understanding interacting autoionizing series.

In this paper we report on a comprehensive study of the Sr $5p_{1/2}ns_{1/2}$ and $5p_{3/2}ns_{1/2}$ $J=1$ states carried out using a multistep-laser excitation method. Our primary goal was the study of the $5p_{1/2}ns_{1/2}$-$5p_{3/2}n's_{1/2}$ interseries interaction which is of interest in dielectronic recombination, the inverse of autoionization.[2] For Sr, dielectronic recombination of Sr^+ and e^- proceeds rapidly through the autoionizing $5pnl$ states. Specifically the process is

$$e^- + Sr^+(5s) \rightarrow Sr(5pnl) \rightarrow Sr(5snl) + h\nu \ .$$

Recently it has been recognized that the fine-structure splitting of the ion, $5p_{1/2}$-$5p_{3/2}$ for Sr^+, may play an important role.[9] For example, in the low Ba $6pnl$ autoionizing states, which are most important for dielectronic recombination, it has been observed[10-12] that there are strong interseries interactions in the $6pnl$ states which lead to autoionization of Ba $6p_{3/2}nl$ states above the $6p_{1/2}$ limit to the Ba^+ $6p_{1/2}$ state and to strong perturbations of the autoionization rates below the $6p_{1/2}$ limit. To assess the generality of this phenomenon requires the study of other atoms. To this end we have undertaken the study of the Sr $5pns$ states reported here. Previously, the $5pns$ autoionizing states of strontium have been studied using single-photon absorption from the ground state.[13,14] Here, by relying on several inherent advantages of the multistep laser excitation method, we are able to determine much more accurately the energies, widths, and channel interaction parameters of the $5pns$ states. Specifically, we have determined the energies and autoionization rates of the unperturbed $5pns$ states and have obtained the perturbed spectra characteristic of the interseries interaction which show that the $5p_{3/2}n's_{1/2}$ states interact with both the $5p_{1/2}ns_{1/2}$ and $5p_{1/2}nd_{3/2}$ series below the $5p_{1/2}$ limit. A novel aspect of the experiment is that we have observed the $5p_{1/2}ns_{1/2}$ states for $n=20$–36 by observing the shakeup satellite features of the $5s20s$-$5p20s$ transition.[15] As previously pointed out, the satellite spectrum is very sensitive to any perturbation of the regularity of the series. In particular, the perturbation produced by the interseries interaction at $n=28$ stands out clearly. In addition, for the first time, interference in the excitation of discrete channels has been unambiguously observed and successfully analyzed using multichannel-quantum-defect theory (MQDT), the channels being the $5p_{1/2}ns_{1/2}$ and $5p_{3/2}n's_{1/2}$ series.

In the sections that follow we describe our experimental approach, the experimental results, the quantum-defect-theory analysis of the data, and the conclusions which may be drawn from the work.

II. EXPERIMENTAL METHOD

Sr atoms were excited to autoionizing states using multistep laser excitation of Sr atoms in conjunction with electron or ion detection. As the method and apparatus

have been described previously,[7,10] this discussion is brief. An effusive atomic Sr beam produced by a resistively heated oven was collimated and passed between a plate and a grid. Its density at the interaction region was 10^8 cm^{-3}. Three laser beams were generated by three Hansch dye-laser oscillator-amplifier systems, which were pumped by the 355 nm third harmonic of a Nd:YAG laser, and gave <1 cm^{-1} linewidth. These three collinear laser beams were linearly polarized and focused to intersect at a right angle with the Sr beam sequentially in time. The excitation scheme is shown in Fig. 1. The first laser was tuned to the Sr resonance line $5s^2\,{}^1S_0$–$5s5p\,{}^1P_1$ at 4609 Å, populating the $^1P_1$ level. The second laser excited the atoms into a Rydberg $5sns\,{}^1S_0$ state, forming a state in which the outer ns electron was on average far from the Sr^+ $5s_{1/2}$ core. When the third laser was scanned in the vicinity of the $5s$-$5pj$ transitions of the Sr^+ ion core, the transition $5sns$-$5pns$ to the autoionizing $5pns$ state was driven. The $5pns$ state quickly decayed to an ion and an electron either of which was detected with a venetian-blind particle multiplier. The output of the particle multiplier went to a gated boxcar averager which then drove an X-Y plotter. As the third laser was scanned through the $5sns$-$5pns$ transition to an unperturbed $5pns$ state a simple Lorentzian line shape was recorded yielding immediately the energy and autoionization width of the $5pns$ state. We note that the radiative decay rates of these Sr $5pns$ states are 10^8 s^{-1}, far less than the observed widths, which are due predominantly to autoionization.

In Sr it happens that the transitions from the $5s5p\,{}^1P_1$ state to the $5s17s$, $5s18s$, $5s16d$, and $5s17d$ states are so close to the Sr^+ $5s_{1/2}$-$5p_{1/2}$ resonance line that the first two lasers alone produced a large background ionization signal in the study of the $17s$ and $18s$ states. To suppress this unwanted background we added a 20 ns optical delay line to the third laser producing a measurable time difference between the background electron signal resulting from the second laser and the desired signal from the third laser. A low dc voltage across the plate and the grid produced a 10 V/cm electric field, directing the electrons through the grid and into the particle detector. The dc electric field was adequate to collect all the electrons and to separate electrons produced by the second and third lasers but did not measurably affect the positions and widths of these $5pns$ states.

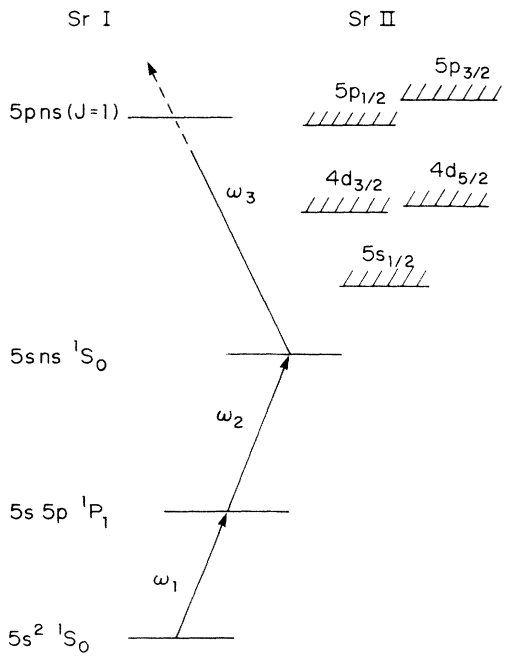

FIG. 1. The excitation scheme for the Sr autoionizing states. The third laser is tuned across the resonance lines of Sr II which is $5s_{1/2}$-$5p_{1/2}$ at 4217Å and $5s_{1/2}$-$5p_{3/2}$ at 4079Å. The dotted section of the ω_3 arrow represents the tuning range of the third laser.

The excitation scans corresponding to the two $J=1$ autoionization series, the $5p_{1/2}ns$ and $5p_{3/2}ns$, were calibrated in frequency with different methods. To calibrate the transitions to the $5p_{1/2}ns_{1/2}$ states we turned the above-mentioned problem to our advantage. As the third laser was scanned across an arbitrary $5s_{1/2}ns_{1/2}$-$5p_{1/2}ns_{1/2}$ transition it also excited the very strong transitions from the $5s5p\,{}^1P$ state to the $5s16d$ and $5s17d$ states and subsequently to the autoionizing $5p_{1/2}16d_j$ and $5p_{1/2}17d_j$ states producing sharp frequency-marker lines at the known $5s5p\,{}^1P_1$–$5snd\,{}^1D_2$ transitions. Unfortunately no natural frequency markers exist for the $5s_{1/2}$-$5p_{3/2}$ transition. Thus the optogalvanic (OG) signal from a hollow cathode Ar discharge lamp was used to calibrate the frequency scale of the third laser with Ar transitions. The OG signal was averaged by a boxcar and recorded on the X-Y plotter simultaneously with the autoionization signal. Additionally a 3.49 cm^{-1} free spectral range etalon followed by a fast photodiode monitored the third laser frequency, providing a measure of the relative frequency difference between the observed states and the frequency markers.

III. EXPERIMENTAL OBSERVATIONS

The energies, widths, and quantum defects of the Sr $5p_jns_{1/2}$ $J=1$ states are given in Tables I and II along with the corresponding values obtained from an MQDT analysis of the data. Figure 2 shows the energy diagram for the $5p_{1/2}ns_{1/2}$ and $5p_{3/2}ns_{1/2}$ states. The quantum defects are obtained from

$$E=I_L-\frac{R_{\mathrm{Sr}}}{(n-\mu)^2}\ , \tag{1}$$

where E is the term energy, I_L is the energy of the ionization limit in question, 69 647.38 cm^{-1} for Sr^+ $5p_{1/2}$ and 70 448.84 cm^{-1} for Sr^+ $5p_{3/2}$, and R_{Sr} is the Rydberg constant for Sr.[16,17] For later use we define the effective quantum number ν by $\nu=n-\mu$.

The $5pns$ states fall into two categories: simple states and the structured states containing information about the $5p_{1/2}ns_{1/2}$-$5p_{3/2}n's_{1/2}$ channel interaction. Simple states have approximately Lorentzian line profiles whereas structured states do not. All the simple states with $n<22$ have been observed in the straightforward manner described in Sec. II and are characterized by Lorentzian peaks from which the widths are apparent and the ener-

TABLE I. Energies, quantum defects, and widths of $5p_{1/2}ns_{1/2}$ states.

n	Experimental energy (cm^{-1})	Quantum defect	Experimental width (cm^{-1})	MQDT calculated energy (cm^{-1})	Calculated width (cm^{-1})
10	67 131.2	3.396	70.2	67 131.4	81.8
11	67 738.0	3.419	35.2	67 737.3	53.4
12	68 166.4	3.392	26.3	68 162.2	35.6
13	68 453.1	3.414	22.3	68 450.6	27.8
14	68 671.8	3.394	16.6	68 670.4	19.5
15	68 829.8	3.415	11.1	68 829.9	15.0
16	68 959.0	3.374	10.7	68 957.4	20.0
17	69 054.9	3.391	9.4	69 053.9	9.2
18	69 132.9	3.395	6.8	69 131.9	7.2
19	69 196.0	3.408	6.6	69 195.4	6.6
20	69 250.1	3.380	6.2	69 249.1	10.4
21	69 294.1	3.375	4.9	69 293.1	4.5
22[a]	69 330.0	3.404	3.6		
23	69 361.5	3.407	3.1		
24	69 388.4	3.416	2.6		
25	69 411.8	3.419	2.4		
26	69 432.1	3.422	2.4		
27	69 449.8	3.431	2.3		
28	69 466.1	3.399	3.0		
29	69 480.0	3.391	1.8		
30	69 492.3	3.395	1.3		
31	69 503.2	3.408	1.2		
32	69 513.2	3.406	1.1		
33	69 522.1	3.405	0.9		
34	69 530.1	3.408	0.9		
35	69 537.4	3.408	0.9		
36	69 544.1	3.408	0.8		

[a]The energy levels of $n \geq 22$ states obtained from sideband excitation are the results of the deconvolution of measured energy peaks with the overlap integral using the MQDT model.

gies are obtained by adding the energy of the center of the observed spectral feature to the energy of the bound $5sns$ state.

In the bound Sr spectrum we are unable to resolve the $5sns$ states and the $5snd$ states for $n \geq 22$ so that it is not possible to observe the $5p_{1/2}ns_{1/2}$ states for $n \geq 22$ in the usual way. To obtain their spectra we recorded the shake-up satellite features of the $5s20s$-$5p_{1/2}20s_{1/2}$ transition. As this has been described in detail elsewhere,[15] we only review here the main theme. The central notion is easily appreciated if we recall that the $5s20s$-$5pns$ transition is the Sr^+ $5s$-$5p$ transition with a spectator electron. In oth-

TABLE II. Energies, quantum defects, and widths of $5p_{3/2}ns_{1/2}$ states.

n	Experimental energy (cm^{-1})	Quantum defect	Experimental width (cm^{-1})	MQDT calculated energy (cm^{-1})	Calculated width (cm^{-1})
10	67 934.1	3.394	68.0	67 918.1	91.5
11	68 539.2	3.419	51.4	68 542.3	56.2
12	68 962.0	3.438	a		
13	69 252.0	3.425	a		
14	69 461.0	3.460	a		
15	69 631.0	3.416	19.2	69 629.9	20.0
16	69 756.6	3.409	17.0	69 753.6	18.1
17	69 853.5	3.423	15.0	69 852.4	14.0
18	69 934.6	3.392	12.3	69 931.3	11.8
19	69 997.8	3.402	9.7	69 995.9	8.5
20	70 051.5	3.381	7.8	70 048.9	7.4
21	70 095.4	3.381	7.0	70 093.1	6.4

[a]The width of the complex spectrum due to channel interaction cannot be derived from the experiment.

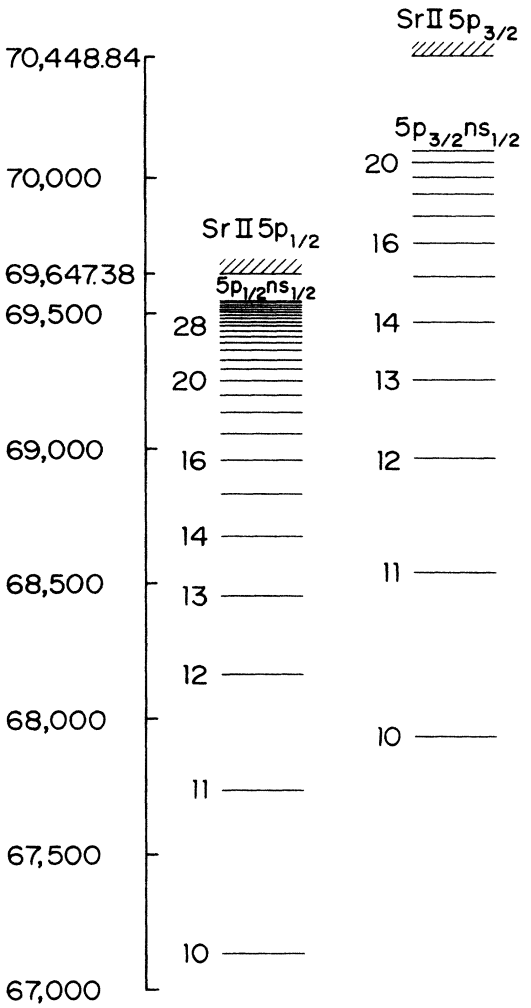

FIG. 2. The energy diagram drawn to scale for the $5p_{1/2}ns$ and $5p_{3/2}ns$ autoionizing series of Sr.

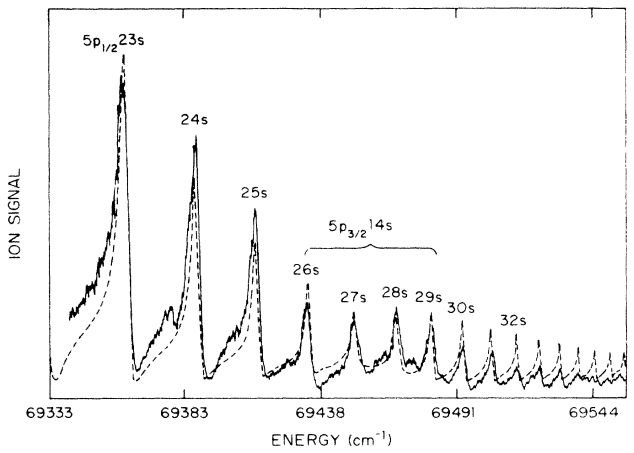

FIG. 3. Shakeup spectrum from the $5s20s$ to the $5p_{1/2}ns_{1/2}$ states. The spectrum extends from 69 333 to 69 544 cm^{-1}, including $5p_{1/2}ns$ states for $n=23$–36. An interference from the excitation of the $5p_{3/2}14s$ state can be observed as a base line change centered at the $6p_{1/2}28s_{1/2}$ state. The data are represented by the solid line and the MQDT analysis is shown as the dashed line.

er words the original $20s$ electron is simply projected onto the final ns state. The strongest transition by far is the $5s20s$-$5p20s$ transition, however it is clear that $5s20s$-$5pns(n\neq 20)$ transitions are also possible, although weaker. The precise form of the satellite shakeup features depends upon the location of the $5pns$ states and the overlap integral which characterizes the $20s$-ns projection of the outer electron.[15] Since the difference in the quantum defects of the $5sns$ and $5pns$ states is small, the $5pns$ states lie near the zeros in the overlap integral, and the quantitative appearance of the spectrum is very sensitive to small changes in the quantum defects of the $5pns$ states. Effectively the *zeros* in the overlap integral provide an internal wavelength scale dependent only on the quantum defect of the initial $5s20s$ state. Against this scale perturbations in energy of the $5p_{1/2}ns_{1/2}$ states stand out clearly.

In Fig. 3 we show the shakeup spectrum obtained when we populated the $5s20s$ state and scanned the third laser to the blue of the $5s20s$-$5p_{1/2}20s_{1/2}$ transition. The $5s20s$ state was chosen because it was the *highest* $5sns$ state which could be excited with only a small amount of excitation of the nearby $5snd$ state. In Fig. 3 the strong satellite features with generally sharp blue sides are quite apparent. In the red wings of the lower satellites appear additional features which are the $5p_{1/2}nd_j$ states reflecting the impurity of our excitation of the $5s20ns$. states. The fact that the satellite features have sharp blue sides indicates immediately that the $5p_{1/2}ns_{1/2}$ states have larger quantum defects that the $5s20s$ state. There is an evident exception to this general rule. At $n=27$–29 we note that the satellite features are quite symmetric and are on top of a higher background signal. This is the location of the perturbing $5p_{3/2}14s_{1/2}$ state. Direct excitation of the $5p_{3/2}14s_{1/2}$ state and interference of this excitation with excitation of the $5p_{1/2}ns_{1/2}$ states for $n=28$ result in the higher background signal and the symmetric $5p_{1/2}ns_{1/2}$ peaks.

To a good approximation the observed spectrum of Fig. 3 is a convolution of the positions and widths of the $5p_{1/2}ns_{1/2}$ states and the overlap integral, thus to extract the positions and widths requires a quantum-defect-theory analysis. If only the excitation to the $5p_{1/2}ns_{1/2}$ channel is included, the background at $n=27$–29 due to the excitation of the $5p_{3/2}14s_{1/2}$ state is not reproduced, nor are the positions of the $n=27$–29 features. When the excitation of the $5p_{3/2}14s_{1/2}$ state is taken into account, including the interference with the $5p_{1/2}ns_{1/2}$ channel, we obtain a simulation in good agreement with the experimental spectrum as shown by Fig. 3. This is to our knowledge the first clear observation of interference between the excitations to series converging to the two limits.

In many cases the energies or quantum defects of the autoionizing states provide only a hint of the interseries interaction which may be present. On the other hand the widths frequently exhibit more noticeable variations.[10] A deviation in the scaled width $\Gamma\nu^3$ is observed to occur at $n=28$ in the $5p_{1/2}$ series although surprisingly not at

$n=20$. However the most dramatic evidence by far of the interseries interaction is the presence of the highly structured $5p_{3/2}ns_{1/2}$ levels below the $5p_{1/2}$ limit. Spectra for the levels, $n=12-14$ exhibit structure due to their coupling with the $5p_{1/2}ns_{1/2}$ and $5p_{1/2}nd_{3/2}$ series. Figures 4–6 show the observed and simulated spectra of the $5p_{3/2}ns$ states for $n=12-14$. This structure is inherent in the $5p_{3/2}ns_{1/2}$ states themselves, it is not an interference of excitation amplitudes.[10] As is easily imagined these spectra represent one of the best probes of the interseries interaction.

In Fig. 4 we show the $5s12s$-$5p_{3/2}12s_{1/2}$ spectrum. The $5p_{1/2}16s_{1/2}$ state produces a Fano $q=0$ feature in the center of the broader $5p_{3/2}12s_{1/2}$ state. Figure 5 is an analogous trace of the $5s13s\ ^1S_0$–$5p_{3/2}13s_{1/2}$ transition which shows the features produced by the $5p_{1/2}20s_{1/2}$ and $5p_{1/2}21s_{1/2}$ states. In this spectrum the $5p_{1/2}20d_{3/2}$ feature is quite prominent. Finally in Fig. 6 we show the $5s14s\ ^1S_0$–$5p_{3/2}14s_{1/2}$ spectrum which is structured by interactions with the $5p_{1/2}26s_{1/2}$-$5p_{1/2}33s_{1/2}$ and $5p_{1/2}26d_{3/2}$-$5p_{1/2}31d_{3/2}$ states. Figures 4–6 are in accord with the theory of Cooke and Cromer[18] which predicts that the $5p_{1/2}ns_{1/2}$ states should lead to $q<0$ features on the red side of a $5p_{3/2}ns_{1/2}$ state, a $q=0$ feature in the center, and $q>0$ features on the blue side. In fact this has already been observed in several other cases.[19,20] The quantum-defect-theory parameters used to obtain all these spectra and the computed values listed in Tables I and II are given in Table III.

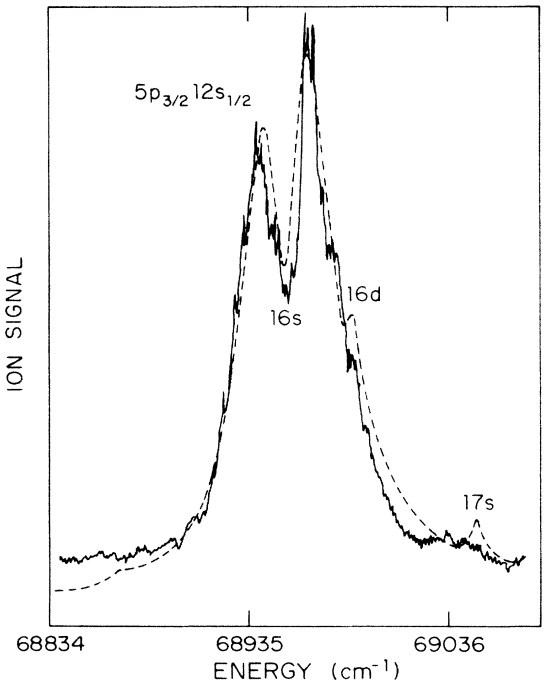

FIG. 4. The $5s12s$-$5p_{3/2}12s_{1/2}$ excitation spectra. Showing the structure imposed by the interacting $5p_{1/2}ns_{1/2}$ and $5p_{1/2}nd_{3/2}$ channels. The structures associated with these states are labeled. The solid curve is the experimental data, and the dashed line is the result of an MQDT simulation.

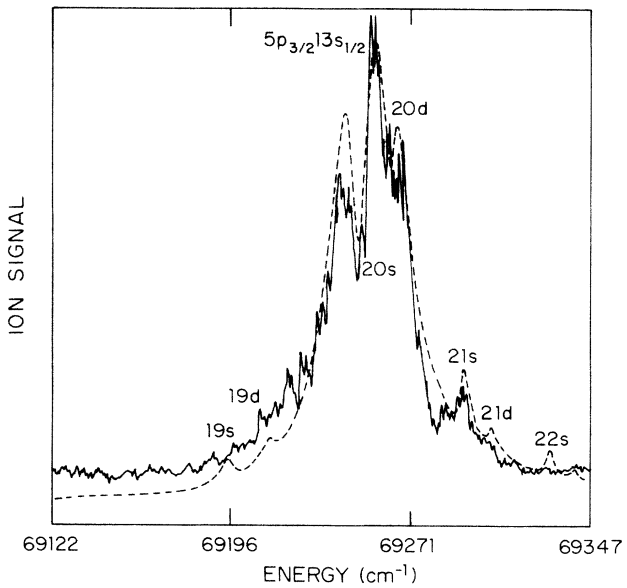

FIG. 5. The $5s13s$-$5p_{3/2}13s_{1/2}$ spectrum showing the interaction with $5p_{1/2}ns_{1/2}$ and $5p_{1/2}nd_{3/2}$ states. The structure attributed to each state is labeled. The solid line is the experimental spectrum and the dashed line is the calculated spectrum.

IV. MQDT ANALYSIS

To describe our experimental results we use a model based on MQDT. Since MQDT analysis of complex spectra is now a well-documented procedure, we only briefly discuss some basic principles here. A channel is defined as a Rydberg series (and its associated continuum) and consists of a well-defined ion core, a Rydberg electron of specified orbital angular momentum and a particular coupling of the ion core and Rydberg electron. A channel wave function ψ_i can be expressed as

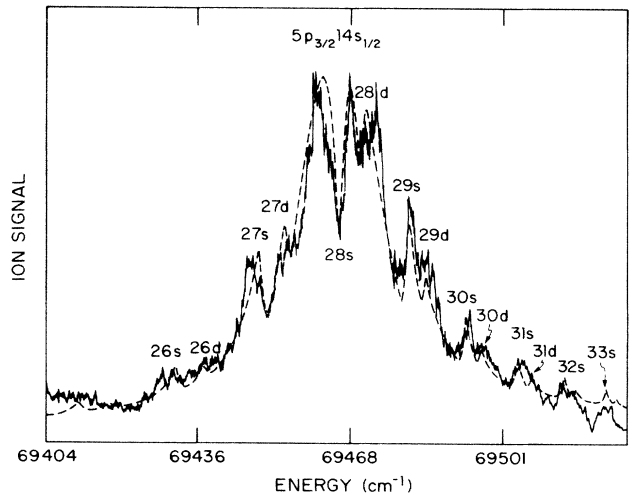

FIG. 6. The $5s14s$-$5p_{3/2}14s_{1/2}$ spectrum showing the structure produced by the high-lying $5p_{1/2}ns_{1/2}$ and $5p_{1/2}nd_{3/2}$ states. The experimental spectrum is shown by a solid line and the calculated spectrum by a dashed line.

TABLE III. MQDT parameters.[a] Quantum defects are only known modulo 1.

μ_1[a]$=3.441$	$R_{12}=0.16$
$\mu_2=3.410$	$R_{13}=0.10$
$\mu_3=2.100$	$R_{14}=0.45$
	$R_{25}=0.40$
	$R_{36}=0.39$

[a]For the $5P_{3/2}12s_{1/2}$ spectrum $\mu_1=3.421$.

$$\psi_i=(c_i f+d_i g)\phi_i \ . \tag{2}$$

Here f and g are the regular and irregular Coulomb basis pair with coefficients c_i and d_i which are fixed by the energy of the Rydberg electron. ϕ_i combines the wave functions of the ion core and of the angular and spin part of the outer electron in the ith channel. The state wave function can be represented as a superposition of the channel functions:

$$\Psi=\sum_i Z_i\psi_i \ . \tag{3}$$

Here the coefficient Z_i reflects the amount of its channel character. The formulation suggested by Cooke and Cromer[18] uses a phase shifted pair of Coulomb functions which allows the intra- and interchannel effects to be treated separately. The MQDT parameters are conveniently divided into two sets; the channel quantum defects μ_i of closed channels which determine the phase of the Rydberg electron for these channels and the interchannel coupling parameters R_{ij} which has zero diagonal elements. In this formulation it is not necessary to specify the absolute phases of the continua thereby reducing the number of parameters. Since in our experiments no information is obtained concerning the absolute phases of the continua, by only their relative phases or phase shifts; we use the phase-shifted basis formulation of Cooke and Cromer.[18]

The requirement of a nondivergent wave function at $r\rightarrow\infty$ leads to the following matrix equation (expressed in terms of the phase-shifted basis)

$$(\underline{\epsilon}+\underline{R})\mathbf{a}=\mathbf{0} \ . \tag{4}$$

Here $\underline{\epsilon}$ and $\underline{R}$ are matrices and $\mathbf{a}$ is a vector. $\underline{\epsilon}$ is diagonal, and the diagonal elements are $\epsilon_i=\tan(\nu_i+\mu_i)$ for bound channels and $\epsilon_i=\tan(-\tau_C)$ for continuum channels of relative phase τ_C. ν_i is the effective quantum number for channel i. The vector solutions a are defined as

$$a_i=Z_i\cos[\pi(\nu_i+\mu_i)] \ . \tag{5}$$

Nontrivial solutions of Eq. (4) require

$$|\underline{\epsilon}+\underline{R}|=0 \tag{6}$$

which represents a polynomial in the continuum ϵ's of a degree equal to the number of continua. Each solution of Eq. (6) provides the different ϵ's, each of which corresponds to one eigenchannel and is used to solve Eq. (4) thereby obtaining a_i and thus Z_i and the state wave function given by Eq. (3). Note that for each eigenchannel all continuum channels are described with the same phase shift.

For an unperturbed series the total autoionization rate is given by the sum of the rates to all allowed continua, e.g., the width Γ_i for channel i is

$$\Gamma_i=\frac{2}{\pi\nu_i^3}\sum_j R_{ij}^2 \ . \tag{7}$$

To analyze the experimental data, we have used a six-channel model which consists of three bound and three continuum channels. The six $J=1$ channels are labeled below: 1, $5p_{3/2}ns_{1/2}$; 2, $5p_{1/2}ns_{1/2}$; 3, $5p_{1/2}nd_{3/2}$; 4, continuum 1; 5, continuum 2; and 6, continuum 3. One can choose the three continuum channels to be orthogonal to each other, so that $R_{45}=R_{46}=R_{56}=0$. From the experimental spectra, it is seen clearly that channel 1 interacts strongly with channel 2, less strongly with channel 3, and there is no obvious indication that channels 2 and 3 interact with each other directly, so we set $R_{23}=0$. For further simplification, we assume that each bound channel is coupled to only one continuum. Thus the only nonzero elements of the R matrix are R_{12}, R_{13}, R_{14}, R_{25}, and R_{36}. These assumptions result in equating seven R-matrix elements to zero.

Estimates for the bound-channel quantum defects can be obtained from the state energies; this procedure works very well for states of channel 1 which lie above the $5p_{1/2}$ ion limit so that channel interaction described here no longer perturbs the energy of these states. Estimates for the R-matrix elements connecting open and closed channels can be made with Eq. (7) using the measured state widths. It is important to note that above the $5p_{1/2}$ ion limit states belonging to channel 1 can autoionize to channels 2 and 3 as well as to channel 4 so that the summation of Eq. (7) must be used. Thus, from the resulting increase in the scaled widths of states in channel 1 as the $5p_{1/2}$ ion limit is surpassed limits on the channel interaction parameters R_{12} and R_{13} can be set. However, to obtain accurate MQDT parameter values and to understand the complex excitation spectra which are obtained below the $5p_{1/2}$ ion limit it is necessary to develop expressions for the state wave functions which can then be used to produce simulations of the spectra in this energy range. Using the methods of Cooke and Cromer[18] we can develop the MQDT wave functions for the region below the $5p_{1/2}$ ion limit.

For our three continuum channel model, Eq. (6) leads to a cubic equation for ϵ_C,

$$\alpha\epsilon_C^3+\beta\epsilon_C^2+\gamma\epsilon_C+\delta=0 \tag{8}$$

(the subscript C indicates continuum), where

$$\alpha=\epsilon_1\epsilon_2\epsilon_3-\epsilon_2R_{13}^2-\epsilon_3R_{12}^2 \ ,$$

$$\beta=R_{25}^2R_{13}^2+R_{12}^2R_{36}^2-R_{25}^2\epsilon_1\epsilon_3-R_{14}^2\epsilon_2\epsilon_3-R_{36}^2\epsilon_1\epsilon_2 \ ,$$

$$\gamma=R_{14}^2R_{25}^2\epsilon_3+R_{25}^2R_{36}^2\epsilon_1+R_{14}^2R_{36}^2\epsilon_2 \ ,$$

$$\delta=-R_{25}^2R_{36}^2R_{14}^2$$

after solving Eq. (8), one obtains three roots, ϵ_{Cj}, for ϵ_C.

To solve Eq. (5) the unit normalization for the three

continuum channels is used; in the present formulation this condition is

$$a_4^2+a_5^2+a_6^2=\frac{1}{1+\epsilon_{Cj}^2} . \tag{9}$$

Using Eqs. (4) and (9) the solution for the state vector a is obtained:

$$a_{1j}^2=\frac{1}{1+\epsilon_{Cj}^2}\left[\left[\frac{R_{14}}{\epsilon_{Cj}}\right]^2+\left[\frac{R_{12}R_{25}}{\epsilon_{Cj}\epsilon_2-R_{25}^2}\right]^2+\left[\frac{R_{13}R_{36}}{\epsilon_{Cj}\epsilon_3-R_{36}^2}\right]^2\right]^{-1},$$

$$a_{2j}=-\frac{\epsilon_{Cj}R_{12}}{\epsilon_2\epsilon_{Cj}-R_{25}^2}a_{1j} ,$$

$$a_{3j}=-\frac{\epsilon_{Cj}R_{13}}{\epsilon_3\epsilon_{Cj}-R_{36}^2}a_{1j} . \tag{10}$$

Finally, the bound part of three independent wave functions is given by

$$\psi_j=\sum_{i=1}^{3}Z_{ij}\phi_i=\sum_{i=1}^{3}\frac{1}{\cos[\pi(\nu_i+\mu_i)]}a_{ij}\phi_i;\quad j=1,2,3 . \tag{11}$$

To calculate the optical cross section for $5sns\ ^1S_0$ Rydberg states to $5p_jns_{1/2}$, $J=1$ autoionizing states we only need to consider the excitation to the bound-channel portion of the wave function because there is no direct continuum excitation in our photoexcitation process. The cross section is given by

$$\sigma=\frac{4\pi^2\omega}{c}\sum_{j=1}^{3}\left|\sum_{i=1}^{3}\langle 5sns\,|\,\mu\,|\,Z_{ij}\phi_i\rangle\right|^2 . \tag{12}$$

Here ω is the angular frequency of the exciting photon and c is the speed of light. As pointed out previously, the excitation method relies on the photoexcitation of the ion core while the Rydberg electron is simply projected onto the new Rydberg wave function of the excited core state. That is,

$$\langle 5sns\,|\,\mu\,|\,\phi_i\rangle=\langle 5s\,|\,\mu\,|\,5_{pj}\rangle\langle ns\,|\,n'l\rangle . \tag{13}$$

With conventional normalization of the wave function per unit energy, the explicit form of the overlap integral is[19]

$$\langle ns\,|\,n'l\rangle=\frac{2\nu'^2\nu^2}{\pi(\nu'^2-\nu^2)}\sin[\pi(\nu'-\nu)]\delta_{l,0} , \tag{14}$$

where ν and ν' are the effective quantum numbers of $5sns$ and $5p_jn's$ states, respectively. By examining Eq. (13) it becomes clear that photoexcitation of $5sns\ ^1S_0$ states to channel 3 ($5p_{1/2}nd_{3/2}$) is negligible due to the angular momentum considerations of the two Rydberg states. Furthermore, one can photoexcite either channel 1 or channel 2 dominantly by creating a large mismatch of the Rydberg-electron shakeup probabilities for the two channels. Generally, the energies and widths of states listed in Tables I and II were obtained by photoexciting the $5sns$ states to $5p_jn's$ states where $n=n'$ so that only one channel is excited. The structured spectrum for the $5p_{3/2}13s_{1/2}$ state was obtained by exciting the $5s13s\ ^1S_0$ state. The $5p_{3/2}14s_{1/2}$ and $5p_{3/2}15s_{1/2}$ spectra were obtained in an analogous fashion. Therefore, these excitation spectra represent the spectral density of channel 1, i.e., Z_1^2. The equation used to obtain the simulations shown in Figs. 4–6 is

$$\sigma=\frac{4\pi^2\omega}{c}\sum_{j=1}^{3}Z_{ij}^2\langle ns\,|\,n's\rangle^2\langle 5s||\mu||5p_j\rangle^2 . \tag{15}$$

In these spectra, the minima in the center *and* the peaks in the wings of the $5p_{3/2}ns_{1/2}$ states correspond to the locations of $5p_{1/2}ns_{1/2}$ and $5p_{1/2}nd_{3/2}$ ($J=1$) states.

As noted above, the energies of $5p_{1/2}n_{1/2}$ states for $n>20$ were obtained from the Rydberg-electron shakeup spectrum which was obtained by preparing the $5s20s\ ^1S_0$ state and scanning with a high-power laser to the blue side of the $5s20s\rightarrow 5p_{1/2}20s_{1/2}$ transition frequency. By this method we obtained satellite features corresponding to $5p_{1/2}ns_{1/2}$ states for $n=21$–36 (as shown in Fig. 3). To account for this shakeup spectrum, excitation into *two* bound channels must be considered. The photoexcitation cross section for $5s20s\rightarrow 5p_{3/2}14s_{1/2}$ and for $5s20s\rightarrow 5p_{1/2}ns_{1/2}$, $n\sim 28$ are comparable due to similar electron shakeup of the Rydberg electron in both cases. Therefore, photoexcitation of the $5s20s$ state to the energy range of the $5p_{3/2}14s_{1/2}$ and $5p_{1/2}28s_{1/2}$ states can occur through both bound channels. The resulting equation for the cross section is thus

$$\sigma=\frac{4\pi^2\omega}{c}\sum_{j=1}^{3}|\langle 5s20s\,|\,\mu\,|\,5p_{3/2}n's\rangle Z_{1j}+\langle 5sns\,|\,\mu\,|\,5p_{1/2}ns\rangle Z_{2j}|^2 . \tag{16}$$

Standard methods of angular momentum algebra allow the reduction of Eq. (16) to

$$\sigma=\frac{4\pi^2\omega}{c}\sum_{j=1}^{3}|\sqrt{2/3}\langle 20s\,|\,n's\rangle Z_{1j}+\sqrt{1/3}\langle 20s\,|\,ns\rangle Z_{2j}|^2|\langle 5s||v||5p\rangle|^2 , \tag{17}$$

where the j dependence in the radial integral is ignored. Using Eq. (17) the simulation in Fig. 3 was obtained. The simulated spectrum was found to be very sensitive to the magnitudes of the MQDT parameters and in addition to the sign of R_{12}. This analysis provided the energies of the $5p_{1/2}ns_{1/2}$ states for $n=21$–35 which are listed in Table I.

V. MQDT PARAMETER VALUES

Applying the theoretical methods of Sec. IV to account for the energies and widths of the autoionizing channels listed in Tables I and II and for complex excitation spectra we obtain the MQDT parameter values given in Table III. The sign of R_{12} is determined to be positive by the

interference in the satellite spectrum of Fig. 3, while the signs of the other R-matrix elements were found to have no effect and were arbitrarily assigned to be positive. Additionally, it was found to be convenient to optimize the quantum defect of channel 1 for the structured $5p_{3/2}12s_{1/2}$ excitation spectrum of Fig. 4. Although the difference is quite small, we used the value given in the footnote of Table III in order to best fit that experimental data.

VI. DISCUSSION

The multistep excitation method complements vacuum ultraviolet (vuv) spectroscopy from the ground state $5s^2$ of Sr I in that it provides much more precise information and, moreover, it allows a purely experimental assignment of the features observed in the vuv spectra.[13,14] In this connection we note that our experiment verifies the assignments made by Connerade *et al.* on the basis of single-configuration Hartree-Fock calculations.[14] The assignments are valuable in providing insight into the relation between the ground and doubly excited state wave functions. In principle the vuv spectra can contain all five odd parity $J=1$ $5pnl$ series, but in fact one strong series is observed converging to each of the $5p_{1/2}$ and $5p_{3/2}$ limits. These series have quantum defects (modulo 1) of 0.45 and 0.54, respectively.[13,14] Additionally, two much weaker series both of quantum defect (modulo 1) 0.2, are observed converging to the $5p_{1/2}$ and $5p_{3/2}$ limits in the higher resolution spectra of Brown *et al.*[13] Based on this work and the work of Connerade *et al.*[14] we can assign the strong series as transitions to the $5pns$ states and the weaker series as transitions to the $5pnd$ states. Assuming that the ground-state wave function for the outer two electrons is given by

$$\Psi_{5s^2}=a(\psi_{5s})^2+b(\Psi_{5p})^2+\cdots , \tag{18}$$

we expect that the transitions to the discrete $5pnl$ states would originate from the $b(\Psi_{5p})^2$ part of the wave function. Propensity rules lead to the expectation that excitation of the $5pnd$ states rather than $5pns$ states would be dominant in contrast to the observations. In any event our experiment and the work of Brown *et al.*[13] clearly show that from the ground state only the $5pns$ states, not the $5pnd$ states, are strongly excited.

As we mentioned in the Introduction, one of the motivations for this work was to investigate the interseries interaction and compare it to that which has been observed in Ba. First we note that the scaled autoionization widths $\Gamma\nu^3$ of the Sr $5pns$ states are large and comparable to the analogous Ba $6pns$ states, illustrating the general facility of the autoionization process when energetically allowed for Rydberg ns states. Specifically in Ba the scaled widths are 1.2×10^4 cm^{-1} and 4×10^4 cm^{-1} for the $6p_{1/2}ns_{1/2}$ and $6p_{3/2}ns_{1/2}$ states[21] while they are 2×10^4 cm^{-1} and 3×10^4 cm^{-1} for the Sr $5p_{1/2}ns_{1/2}$ and $5p_{3/2}ns_{1/2}$ states. In addition, the $p_{1/2}ns$-$p_{3/2}n's$ MQDT interaction parameters R_{12} of Sr and Ba are also quite comparable being 0.16 and 0.17, respectively. Because this interaction results from the short-range electron-ion core scattering, our data indicate that the short-range electron correlation effects are of the same magnitude for both Sr and Ba. Similar values of related channel interaction parameters for the alkaline earths Ca, Sr, Ba, and Ra have been observed previously for the bound odd-parity states.[22,23]

In addition, the coupling strengths in Sr and Ba between $p_{3/2}ns_{1/2}$ states to $p_{1/2}nd$ states are both large; however, the interaction is significantly stronger in Ba. In terms of the quantum-defect-theory parameters the values of R_{13} are 0.10 for Sr and 0.42 for Ba.[24] The $5p_{1/2}nd_{3/2}$ and $5p_{3/2}ns_{1/2}$ channel interaction can come from two terms; the direct quadrupole coupling is one, and a short-range electron correlation of the two electrons is the other. For both Sr and Ba the total effects from these two terms are substantial, however, the relative contributions of these effects remains experimentally undetermined and will most likely await sophisticated calculations.

VII. CONCLUSION

In this report we have presented the results of an extensive series of measurements of the autoionizing Sr $5p_{1/2}ns_{1/2}$ and $5p_{3/2}ns_{1/2}$ $J=1$ states. The observations, consisting of energies and widths of the autoionizing states as well as the complex spectra produced by interseries interaction, can all be reduced to a few physically meaningful parameters using a six-channel MQDT analysis of the data. These measurements allow the assignment of configurations in existing vuv spectra turning them into a well-posed problem ripe for theoretical attack. The measurement also shows that the interseries $5p_{1/2}ns_{1/2}$ and $5p_{3/2}ns_{1/2}$ interaction has similar strength in Sr and Ba, which implies that the electron correlation effects for small radial extensions are comparable in both elements.

ACKNOWLEDGMENTS

This work was supported by the U.S. Department of Energy (Division of Chemical Sciences, Office of Basic Energy Sciences) under Grant No. DE-FG05-85ER13394. It is a pleasure to acknowledge useful discussions with H. P. Kelly in the course of this work.

[1]S. E. Harris, Opt. Lett. **5**, 1 (1980).
[2]A. Burgess, Astrophys. J. **139**, 776 (1964).
[3]H. P. Kelly, in *Atomic Physics 8*, edited by I. Lindgren, A. Rosen, and S. Svanberg (Plenum, New York, 1983).
[4]M. Ya. Amusia and N. A. Cherepkov, Case Stud. At. Phys. **5**, 47 (1975).
[5]M. J. Seaton, Proc. Phys. Soc. London **88**, 801 (1966).
[6]U. Fano, Phys. Rev. A **2**, 353 (1970).
[7]W. E. Cooke, T. F. Gallagher, S. A. Edelstein, and R. M. Hill, Phys. Rev. Lett. **40**, 178 (1978).
[8]U. Fano, Phys. Rev. **124**, 1866 (1961).
[9]L. J. Rozman, in *Physics of Electron and Atom Collision*, edited by S. Datz (North-Holland, Amsterdam, 1982).
[10]F. Gounand, T. F. Gallagher, W. Sandner, K. A. Safinya, and

R. Kachru, Phys. Rev. A **27**, 1925 (1983).
[11]W. E. Cooke and S. A. Bhatti, Phys. Rev. A **26**, 391 (1982).
[12]O. C. Mullins, Y. Zhu, E. Y. Xu, and T. F. Gallagher, Phys. Rev. A **32**, 2234 (1985).
[13]C. M. Brown, M. S. Longmire, and M. L. Ginter, J. Opt. Soc. Am. **73**, 985 (1983).
[14]J. P. Connerade M. A. Baig, W. R. S. Garton, and G. H. Newson, Proc. R. Soc. London Ser. A **371**, 295 (1980).
[15]N. H. Tran, P. Pillet, R. Kachru, and T. F. Gallagher, Phys. Rev. A **29**, 2640 (1984).
[16]P. Esherick, Phys. Rev. A **15**, 1920 (1977).
[17]C. E. Moore, *Atomic Energy Levels,* NBS Circular No. 467 (U.S. GPO, Washington, D.C., 1949).
[18]W. E. Cooke and C. L. Cromer, Phys. Rev. A **32**, 2752 (1985).
[19]S. A. Bhatti, C. L. Cromer, and W. E. Cooke, Phys. Rev. A **24**, 161 (1981).
[20]S. M. Jaffe, R. Kachru, H. B. van Linden van der Heuvell, and T. F. Gallagher, Phys. Rev. A **32**, 1480 (1985).
[21]W. E. Cooke (unpublished).
[22]J. A. Armstrong, J. J. Wynne, and P. Esherick, J. Opt. Soc. Am. **69**, 211 (1979).
[23]J. J. Wynne and J. A. Armstrong, IBM J. Res. Dev. **23**, 490 (1979).
[24]S. A. Bhatti, Ph.D. thesis, University of Southern California, 1983 (unpublished).